The Stannides RE_2Ni_2Sn (RE = Pr, Ho, Er, Tm) – Structural Transition from the W_2B_2Co to the Mo_2B_2Fe Type as a Function of the Rare Earth Size

Birgit Heying[a], Ute Ch. Rodewald[a], Bernard Chevalier[b], and Rainer Pöttgen[a]

[a] Institut für Anorganische und Analytische Chemie, Universität Münster, Corrensstrasse 30, 48149 Münster, Germany

[b] CNRS, Université de Bordeaux, ICMCB, 87 Avenue Dr. A. Schweitzer, F-33608 Pessac-Cedex, France

Reprint requests to R. Pöttgen. E-mail: pottgen@uni-muenster.de

Z. Naturforsch. **2013**, *68b*, 10 – 16 / DOI: 10.5560/ZNB.2013-2296
Received November 19, 2012

The stannides RE_2Ni_2Sn (RE = Pr, Ho, Er, Tm) were synthesized by arc-melting of the elements and characterized by powder X-ray diffraction. Pr_2Ni_2Sn crystallizes with the orthorhombic W_2B_2Co-type structure, *Immm*, $a = 443.8(1)$, $b = 572.1(1)$, $c = 855.1(2)$ pm, $wR2 = 0.0693$, 293 F^2 values, 13 variables. A structural transition to the tetragonal Mo_2B_2Fe type occurs for the heavier rare earth elements. The structures of Ho_2Ni_2Sn ($a = 729.26(9)$, $c = 366.66(7)$ pm, $wR2 = 0.0504$, 250 F^2 values, 12 variables), Er_2Ni_2Sn ($a = 727.2(2)$, $c = 364.3(1)$ pm, $wR2 = 0.0397$, 262 F^2 values, 12 variables), and Tm_2Ni_2Sn ($a = 725.2(1)$, $c = 362.8(1)$ pm, $wR2 = 0.0545$, 258 F^2 values, 12 variables) were refined from single-crystal diffractometer data. The switch in structure type is driven by the size of the rare earth element. The $[Ni_2Sn]$ substructures are composed of Ni_2Sn_2 squares and Ni_4Sn_2 hexagons in Pr_2Ni_2Sn, and of Ni_3Sn_2 pentagons in Er_2Ni_2Sn. The Ni_4Sn_2 hexagons and Ni_3Sn_2 pentagons exhibit Ni_2 pairs with Ni–Ni distances of 247 pm in Pr_2Ni_2Sn, and of 250 pm in Er_2Ni_2Sn.

Key words: Stannides, Crystal Structure, Lanthanoid Contraction

Introduction

The ternary rare earth (RE) compounds of the general composition RE_2T_2X (T = electron-rich transition metal; X = Mg, Zn, Cd, Al, Ga, In, Sn, Pb) crystallize with three different structure types, depending on the size of the atoms and the valence electron concentration (VEC): (i) the tetragonal Mo_2B_2Fe type, space group *P4/mbm* [1] (a ternary ordered version of the U_3Si_2 structure), (ii) the orthorhombic Mn_2B_2Al type [2], space group *Cmmm*, and (iii) the orthorhombic Co_2B_2W type [3], space group *Immm*. Most representatives occur for the Mo_2B_2Fe type [4]. The common structural motif of these three structure types are transition metal-centered trigonal prisms. Exemplarily we present projections of the Pr_2Ni_2Sn, Er_2Ni_2Sn, and Er_2Ni_2Pb [5] structures in Fig. 1.

Several series of the RE_2T_2X intermetallics show structural transitions as a function of the rare earth element (lanthanoid contraction) or the chemical composition. If the radii criteria do not match for a Mo_2B_2Fe-type structural arrangement, superstructure formation with small distortions is possible. This has first been observed for the ternary stannides Er_2Au_2Sn [6] and U_2Pt_2Sn [7]. Other compounds show the formation of defects on the transition metal site, *e. g.* $RE_2Ni_{2-x}Cd$ [8, 9] and $RE_2Ni_{2-x}In$ [10]. In case of the indides, the phases with a nickel defect crystallize with the tetragonal Mo_2B_2Fe type, while those with the ideal composition adopt the orthorhombic Mn_2B_2Al structure. The cadmium compounds [9] crystallize with a tetragonal Mo_2B_2Fe type and an orthorhombic Mn_2B_2Al type, respectively, in the low- and the high-temperature modification. This phase transition is of reconstructive nature.

In continuation of our systematic studies of RE_2T_2X intermetallics we have recently investigated the RE_2Ni_2Sn series with the heavier rare earth elements. The representatives with the early rare earth elements [11 – 32] crystallize with the W_2B_2Co-type structure. Especially Ce_2Ni_2Sn [12 – 14, 16 – 18, 22 – 24, 26, 27] has intensively been studied. This stan-

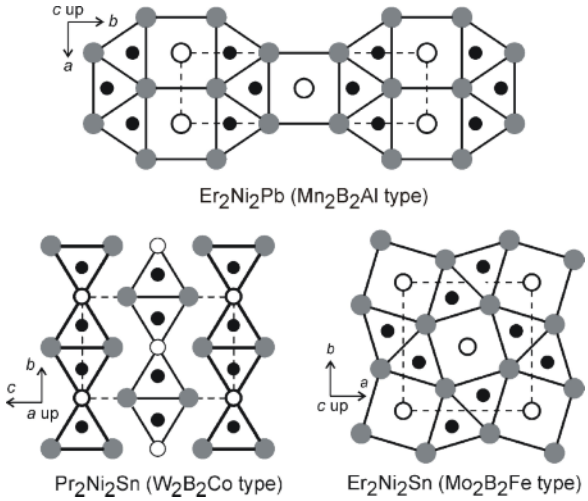

Fig. 1. Projections of the Pr_2Ni_2Sn, Er_2Ni_2Sn, and Er_2Ni_2Pb structures along the short unit cell axis. Rare earth, nickel and tin (or lead) atoms are drawn as medium grey, black filled, and open circles, respectively. The trigonal prismatic slabs around the nickel atoms are emphasized.

nide behaves like a Kondo system and orders antiferromagnetically at $T_N = 4.7$ K. Above T_N, Ce_2Ni_2Sn shows a large negative magnetoresistance ($\cong -20\,\%$ at 6 K and for an applied magnetic field of 9 T) mainly due to the Kondo effect.

The smallest rare earth element for which the W_2B_2Co-type structure is realized is dysprosium. Our current studies have revealed a switch in structure type from Ho_2Ni_2Sn on. The ternary holmium, erbium and thulium stannides reported herein crystallize with the tetragonal Mo_2B_2Fe type, similar to Lu_2Ni_2Sn [31]. Furthermore we obtained the new stannide Pr_2Ni_2Sn with the W_2B_2Co type.

Experimental

Synthesis

Starting materials for the syntheses of the RE_2Ni_2Sn stannides were sublimed pieces of the rare earth metals (Kelpin, Chempur, or smart elements, $> 99.9\,\%$), nickel wire (Alfa-Aesar, $\varnothing$ 1 mm, $> 99.5\,\%$), and tin granules (Merck, $> 99.9\,\%$). Pr_2Ni_2Sn was obtained by arc-melting [33] pieces of the three elements under an argon atmosphere of *ca.* 700 mbar. The argon was purified over titanium sponge (900 K), silica gel, and molecular sieves. The arc-melted button was sealed in an evacuated silica tube and annealed at 1070 K for one week. Synthesis attempts for RE_2Ni_2Sn with RE = Ho, Er, and Tm with the ideal starting 2 : 2 : 1 composition resulted in considerable amounts of the equiatomic RENiSn phases (orthorhombic TiNiSi type) as by-products. No RE_2Ni_2Sn single crystals were obtained. After inspection of the RE-Ni-Sn phase diagrams with RE = Y [32], Nd [28], Gd [30], Dy [29], and Lu [31] we used the starting compositions $42RE : 40Ni : 18Sn$ for the heavy rare earth elements. After arc-melting these samples we obtained the missing RE_2Ni_2Sn stannides. Only trace amounts of the RENiSn phases were evident. The RE_2Ni_2Sn stannides are air stable over months.

EDX data

Semiquantitative EDX analyses of the single crystals studied on the diffractometers were carried out in variable pressure mode with a Zeiss EVO® MA10 scanning electron microscope with the rare earth trifluorides, nickel, and tin as standards. The experimentally observed average compositions were close to the ideal ones. No impurity elements were detected.

X-Ray diffraction

All polycrystalline RE_2Ni_2Sn samples were characterized by powder X-ray diffraction using the Guinier technique: imaging plate detector, Fujifilm BAS-1800, Cu$K_{\alpha 1}$ radiation and α-quartz ($a = 491.30$, $c = 540.46$ pm) as an internal standard. The lattice parameters (Table 1) were refined from the Guinier powder data using a standard least-squares routine. The experimental patterns were compared to calculated ones [34] in order to assure correct indexing.

Small single crystals of Pr_2Ni_2Sn were selected from the crushed annealed sample, while those of Ho_2Ni_2Sn, Er_2Ni_2Sn, and Tm_2Ni_2Sn were taken directly from the arc-melted samples. The crystals were glued to quartz fibers using beeswax and characterized on a Buerger camera (using white Mo radiation) to check their quality. The intensity data collection from suitable Pr_2Ni_2Sn, Er_2Ni_2Sn, and Tm_2Ni_2Sn crystals was performed on a Stoe IPDS-II image plate system (graphite-monochromatized MoK_α radiation; $\lambda = 71.073$ pm) in oscillation mode. The Ho_2Ni_2Sn data set was measured on a Stoe Stadi Vari diffractometer equipped with a Mo micro focus source and a Pilatus detection system and scaled subsequently according to the Gaussian-shaped profile of the X-ray source. Numerical absorption corrections were applied to all data sets. Details about the data collections and the crystallographic parameters are summarized in Table 2.

Structure refinements

Isotypism of Pr_2Ni_2Sn with W_2B_2Co and of RE_2Ni_2Sn (RE = Ho, Er, Tm) with Mo_2B_2Fe was already evident

Table 1. Lattice parameters (Guinier powder data) of RE_2Ni_2Sn compounds. Standard deviations are given in parentheses.

Compound	Structure type	Space group	a (pm)	b (pm)	c (pm)	V (nm^3)	Reference
Sc_2Ni_2Sn	Mo_2FeB_2	*P4/mbm*	709.28(4)	*a*	338.00(3)	0.1700	[11]
Y_2Ni_2Sn	W_2CoB_2	*Immm*	425.7(2)	558.5(2)	835.1(4)	0.1985	[32]
Ce_2Ni_2Sn	W_2CoB_2	*Immm*	439.1(2)	573.0(3)	858.6(4)	0.2160	[27]
Ce_2Ni_2Sn	W_2CoB_2	*Immm*	439.1(1)	573.5(2)	859.1(3)	0.2163	[13]
Ce_2Ni_2Sn	W_2CoB_2	*Immm*	439.36(9)	573.96(9)	859.67(13)	0.2168	[12]
Pr_2Ni_2Sn	W_2CoB_2	*Immm*	438.0(1)	572.1(1)	855.1(2)	0.2171	this work
Nd_2Ni_2Sn	W_2CoB_2	*Immm*	436.2(2)	570.1(3)	850.3(5)	0.2114	[27]
Nd_2Ni_2Sn	W_2CoB_2	*Immm*	436.0(1)	569.5(2)	849.8(2)	0.2110	[14]
Nd_2Ni_2Sn	W_2CoB_2	*Immm*	435.8(2)	569.2(1)	849.5(3)	0.2107	[28]
Sm_2Ni_2Sn	W_2CoB_2	*Immm*	432.1(3)	567.0(3)	841.8(4)	0.2070	[27]
Gd_2Ni_2Sn	W_2CoB_2	*Immm*	429.1(3)	563.2(4)	839.1(7)	0.2028	[27]
Gd_2Ni_2Sn	W_2CoB_2	*Immm*	429.4(1)	563.8(1)	839.0(1)	0.2031	[20]
Tb_2Ni_2Sn	W_2CoB_2	*Immm*	427.7(3)	560.9(4)	832.3(5)	0.1996	[27]
Tb_2Ni_2Sn	W_2CoB_2	*Immm*	427.8(1)	561.4(1)	833.2(1)	0.2001	[20]
Dy_2Ni_2Sn	W_2CoB_2	*Immm*	424.7(1)	561.5(1)	827.3(1)	0.1973	[20]
Ho_2Ni_2Sn	Mo_2FeB_2	*P4/mbm*	729.26(9)	*a*	366.66(7)	0.1950	this work
Er_2Ni_2Sn	Mo_2FeB_2	*P4/mbm*	727.2(2)	*a*	364.3(1)	0.1927	this work
Tm_2Ni_2Sn	Mo_2FeB_2	*P4/mbm*	725.2(1)	*a*	362.8(1)	0.1908	this work
Lu_2Ni_2Sn	Mo_2FeB_2	*P4/mbm*	723.8(3)	*a*	360.2(1)	0.1887	[31]

Table 2. Crystal data and structure refinement results for the stannides RE_2Ni_2Sn.

Compound	Pr_2Ni_2Sn	Ho_2Ni_2Sn	Er_2Ni_2Sn	Tm_2Ni_2Sn
Space group, Z	*Immm*, 2	*P4/mbm*, 2	*P4/mbm*, 2	*P4/mbm*, 2
Structure type	W_2B_2Co	Mo_2B_2Fe	Mo_2B_2Fe	Mo_2B_2Fe
Molar mass, g mol^{-1}	517.93	565.97	570.63	573.97
Calculated density, g cm^{-3}	7.92	9.64	9.84	9.99
Absorption coefficient, mm^{-1}	36.0	55.6	58.8	61.9
F(000), e	448	480	484	488
Crystal size, μm^3	$10 \times 20 \times 40$	$20 \times 20 \times 90$	$10 \times 40 \times 50$	$10 \times 30 \times 60$
Transm. ratio (max / min)	0.782 / 0.379	0.474 / 0.211	0.593 / 0.125	0.502 / 0.218
Diffraktomer	IPDSII	StadiVari	IPDSII	IPDSII
X-Ray source, Mo	sealed tube	GeniX^{3D}	sealed tube	sealed tube
Detector	Imaging Plate	PILATUS 100K	Imaging Plate	Imaging Plate
Detector distance, mm	60	70	60	60
Exposure time, sec	600	12	600	300
ω range increment, deg	1.0	0.3	1.0	1.0
Integr. parameter A, B, EMS	12.8, 3.0, 0.012	7.3, −5.3, 0.013	13.0, 3.0, 0.012	12.9, 3.0, 0.012
θ range, deg	4–35	4–34	4–35	4–35
Range in *hkl*	±7, ±9, ±13	±11, ±11, ±5	±11, ±11, +5	±11, ±11, ±5
Total no. reflections	1736	2823	1584	2847
Independent reflections / R_{int}	293 / 0.0728	250 / 0.0363	262 / 0.0119	258 / 0.0487
Reflections with $I > 2\sigma(I)/R_\sigma$	243 / 0.0476	220 / 0.0214	256 / 0.0092	234 / 0.0206
Data / parameters	293 / 13	250 / 12	245 / 12	258 / 12
Goodness-of-fit on F^2	0.994	1.017	1.341	1.164
$R1$ / $wR2$ for $I > 2\sigma(I)$	0.0303 / 0.0656	0.0211 / 0.0499	0.0180 / 0.0389	0.0254 / 0.0530
$R1$ / $wR2$ for all data	0.0417 / 0.0693	0.0244 / 0.0504	0.0208 / 0.0397	0.0317 / 0.0545
Extinction coefficient	0.0041(9)	0.0057(8)	0.0027(4)	0.0033(7)
Largest diff. peak / hole, e Å^{-3}	2.10 / −2.40	1.66 / −1.73	2.11 / −1.36	2.38 / −3.34

from the Guinier powder data. The systematic extinctions of the data sets were compatible with space groups *Immm* and *P4/mbm*, respectively. The atomic parameters of orthorhombic Ce_2Ni_2Sn [12] and tetragonal Ce_2Pt_2In [35] were taken as starting values, and the four structures were refined with anisotropic displacement parameters for all atoms with SHELXL-97 (full-matrix least-squares on F_o^2) [36, 37]. Since the crystals of the RE_2Ni_2Sn stannides with the heavy rare earth elements were taken from samples of the starting compositions 42RE : 40Ni : 18Sn, the occupancy parameters were refined in separate series of least-squares cycles for all data sets. All sites were fully occupied within two

Table 3. Atomic coordinates and isotropic displacement parameters (pm^2) of RE_2Ni_2Sn compounds. $U_{13} = U_{23} = 0$. U_{eq} is defined as one third of the trace of the orthogonalized U_{ij} tensor.

Atom	Wyckoff position	x	y	z	U_{11}	U_{22}	U_{33}	U_{12}	U_{eq}
Pr_2Ni_2Sn									
Pr	4*j*	1/2	0	0.29695(8)	145(3)	117(3)	116(3)	0	126(2)
Ni	4*h*	0	0.2156(3)	1/2	158(7)	208(8)	149(7)	0	172(3)
Sn	2*a*	0	0	0	128(5)	106(4)	125(4)	0	120(2)
Ho_2Ni_2Sn									
Ho	4*h*	0.17493(4)	1/2+*x*	1/2	137(2)	U_{11}	119(2)	−11(1)	131(2)
Ni	4*g*	0.37885(14)	1/2+*x*	0	172(4)	U_{11}	164(6)	−26(4)	169(3)
Sn	2*a*	0	0	0	123(3)	U_{11}	172(5)	0	139(2)
Er_2Ni_2Sn									
Er	4*h*	0.17434(3)	1/2+*x*	1/2	107(1)	U_{11}	89(2)	−13(1)	101(1)
Ni	4*g*	0.37864(12)	1/2+*x*	0	137(3)	U_{11}	133(5)	−25(4)	136(2)
Sn	2*a*	0	0	0	90(2)	U_{11}	139(3)	0	106(2)
Tm_2Ni_2Sn									
Tm	4*h*	0.17403(5)	1/2+*x*	1/2	113(2)	U_{11}	88(2)	−11(2)	105(2)
Ni	4*g*	0.37843(17)	1/2+*x*	0	143(5)	U_{11}	134(6)	−26(5)	140(3)
Sn	2*a*	0	0	0	97(3)	U_{11}	132(4)	0	109(2)

standard deviations, and the ideal compositions were assumed again in the following cycles. The final difference Fourier syntheses revealed no residual peaks. The refined atomic positions, equivalent isotropic displacement parameters, and interatomic distances (exemplarily for Pr_2Ni_2Sn and Er_2Ni_2Sn) are given in Tables 3 and 4.

Further details of the crystal structure investigations may be obtained from Fachinformationszentrum Karlsruhe, 76344 Eggenstein-Leopoldshafen, Germany (fax: +49-7247-808-666; E-mail: crysdata@fiz-karlsruhe.de, http://www.fiz-karlsruhe.de/request_for_deposited_data.html) on quoting the deposition number CSD-425429 (Pr_2Ni_2Sn), CSD-425430 (Ho_2Ni_2Sn), CSD-425431 (Er_2Ni_2Sn), and CSD-425432 (Tm_2Ni_2Sn).

Table 4. Interatomic distances (pm) of Pr_2Ni_2Sn and Er_2Ni_2Sn, calculated with the powder lattice parameters. Standard deviations are all equal or less than 0.2 pm.

Pr_2Ni_2Sn				Er_2Ni_2Sn			
Pr:	2	Ni	301.6	Er:	2	Ni	278.1
	4	Ni	307.6		4	Ni	284.4
	2	Sn	334.6		4	Sn	324.6
	2	Sn	337.2		1	Er	358.6
	1	Pr	347.3		2	Er	364.3
	4	Pr	370.8		4	Er	379.9
Ni:	1	Ni	246.7	Ni:	1	Ni	249.6
	2	Sn	275.2		2	Er	278.1
	2	Pr	301.6		4	Er	284.4
	4	Pr	307.6		2	Sn	289.1
Sn:	4	Ni	275.2	Sn:	4	Ni	289.1
	4	Pr	334.6		8	Er	324.6
	4	Pr	337.2				

Discussion

The series of RE_2Ni_2Sn stannides has been completed with the synthesis of the members with praseodymium, holmium, erbium, and thulium as rare earth elements. Our own phase-analytical studies gave no hint for the formation of a corresponding lanthanum compound. This is in full agreement with the phase analytical studies of Zhuang *et al.* [38]. Also no such compounds form with europium and ytterbium, since these two elements prefer divalent oxidation states. The course of the unit cell volumes is presented in Fig. 2. In agreement with the lanthanoid contraction the volume decreases from Ce_2Ni_2Sn to Lu_2Ni_2Sn. The plot shows no anomaly for the cerium compound, in accord with the trivalent ground state accompanied by magnetic ordering at $T_N = 4.7$ K [12 – 14, 16 – 18, 22 – 24, 26, 27]. The volume of Y_2Ni_2Sn fits in between Tb_2Ni_2Sn and Dy_2Ni_2Sn, similar to examples of several other 2-2-1 series [4]. Sc_2Ni_2Sn shows by far the smallest cell volume in the RE_2Ni_2Sn series.

From Dy_2Ni_2Sn to Ho_2Ni_2Sn we observed a switch from the orthorhombic W_2B_2Co- [3] to the tetragonal Mo_2B_2Fe-type [1] structure. This structural transition has drastic influences on the near-neighbor coordination of the atoms. The coordination polyhedra for Pr_2Ni_2Sn and Er_2Ni_2Sn are presented in Fig. 3. If one considers only the nickel-tin coordination (these atoms have the shortest distances to the rare earth elements), Pr_2Ni_2Sn shows coordination of Pr by

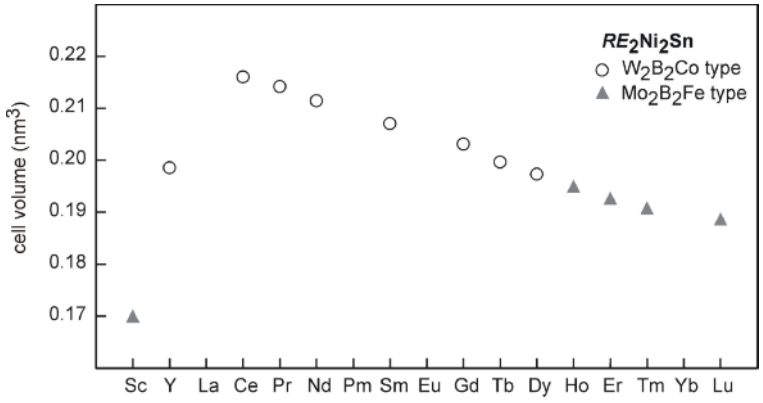

Fig. 2. Course of the cell volumes in the series of RE_2Ni_2Sn compounds.

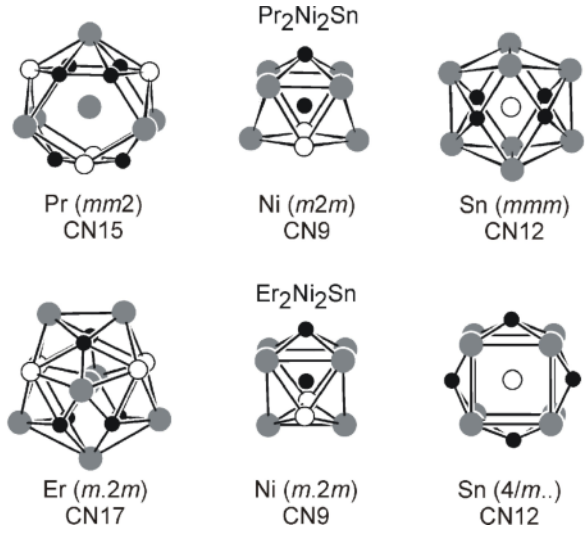

Fig. 3. The coordination polyhedra in the structures of Pr_2Ni_2Sn and Er_2Ni_2Sn. Rare earth, nickel and tin atoms are drawn as medium grey, black filled and open circles, respectively. Site symmetries are indicated.

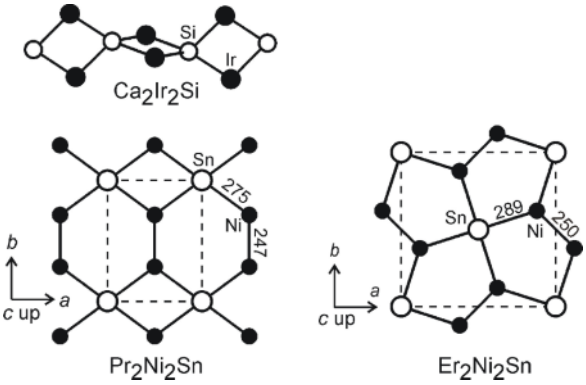

Fig. 4. The $[Ni_2Sn]$ substructures in Pr_2Ni_2Sn and Er_2Ni_2Sn. Nickel and tin atoms are drawn as black filled and open circles, respectively. Relevant interatomic distances are indicated. The $[Ir_2Si]$ substructure of Ca_2Ir_2Si is shown for comparison.

a Ni_4Sn_2 hexagon and a Ni_2Sn_2 square, while Er in Er_2Ni_2Sn has two parallel Ni_3Sn_2 pentagons in the first coordination shell. Er_2Ni_2Sn has two more rare earth atoms in its coordination shell as compared to Pr_2Ni_2Sn (Table 4). The nickel atoms in both stannides have coordination number 9 in the form of tricapped trigonal prisms. The tin atoms in Pr_2Ni_2Sn and Er_2Ni_2Sn have four nickel and eight rare earth neighbors, but with different site symmetry.

The shortest interatomic distances in both structures occur for the nickel atoms, which form pairs with Ni–Ni distances of 247 pm in Pr_2Ni_2Sn and 250 pm in Er_2Ni_2Sn (Table 4), close to the Ni–Ni distance of 249 pm in *fcc* nickel [39]. Each nickel atom coordinates to two tin atoms, leading to the $[Ni_2Sn]$ substructures with four-, five-, and six-membered rings as presented in Fig. 4. The tin atoms have square-planar $SnNi_4$ coordination with Ni–Sn distances of 289 pm in Er_2Ni_2Sn, but a planar $SnNi_4$ rectangle in Pr_2Ni_2Sn with a distance of 275 pm for Ni–Sn. These Ni–Sn distances are all significantly longer than the sum of the covalent radii of 255 pm [40]. Especially for Er_2Ni_2Sn the Ni–Sn bonding is weak and will not significantly contribute to the overall stability of the structure. Nevertheless, this weakness (in comparison with Pr_2Ni_2Sn) is compensated by short Er–Ni distances of 278 and 284 pm, close to the sum of the covalent radii of 272 pm [40].

A third structure type (HT-Pr_2Co_2Al [41, 42] and Ca_2Ir_2Si [43]) exists for the 2-2-1 composition, how-

ever, with another polyanionic substructure. As an example we present the [Ir_2Si] substructure of Ca_2Ir_2Si in Fig. 4. The silicon atoms have four nearest iridium neighbors in strongly distorted tetrahedral coordination within the one-dimensional polyanion. Flattening of these chains followed by condensation through T–T bonding leads to the substructure of the W_2B_2Co type. Indeed, Pr_2Co_2Al is dimorphic with a W_2B_2Co-type low-temperature modification and a monoclinic (space group $C2/c$) high-temperature modification.

The orthorhombic structure type W_2B_2Co exists for a small range of valence electron concentrations (VEC) from 26 (*e. g.* Ca_2Pt_2Cd [44]) to 30 (Pr_2Ni_2Sn [this work]), while a slightly larger VEC range from 26 (*e. g.* La_2Rh_2Cd [45]) to 32 (*e. g.* Er_2Au_2Sn [6]) applies to the Mo_2B_2Fe-type compounds. This is probably related to the larger number of representatives [4] for the latter type. Both structure types have flexibility for the geometry within the planar polyanionic layers, accounting for the difference in size and electronegativity, as is evident from electronic structure calculations on Ca_2Pt_2Cd [44] and Ca_2Cu_2Ga [46].

Similar to the series of equiatomic stannides *RE*NiSn [47], *RE*PdSn [48], *RE*AgSn [49], and *RE*PtSn [50], one might think of high-temperature or high-pressure modifications for those rare earth elements, where the transition in structure type takes place. Careful inspection of the Guinier powder diagrams of the melted and quenched Ho_2Ni_2Sn samples gave no hint for a W_2B_2Co-type high-temperature modification. We have therefore planned high-pressure high-temperature studies on Dy_2Ni_2Sn, expecting to find a Mo_2B_2Fe-type high-pressure modification. Since the whole RE_2Ni_2Sn series has the same VEC, the switch in structure types is most likely driven by the course of the lanthanoid contraction.

Acknowledgement

This work was supported by the Deutsche Forschungsgemeinschaft.

[1] W. Rieger, H. Nowotny, F. Benesovsky, *Monatsh. Chem.* **1964**, *95*, 1502.
[2] H. J. Becher, K. Krogmann, E. Peisker, *Z. Anorg. Allg. Chem.* **1996**, *344*, 140.
[3] W. Rieger, H. Nowotny, F. Benesovsky, *Monatsh. Chem.* **1966**, *97*, 378.
[4] M. Lukachuk, R. Pöttgen, *Z. Kristallogr.* **2003**, *218*, 767.
[5] L. D. Gulay, D. Kaczorowski, M. Wolcyrz, *J. Alloys Compd.* **2000**, *311*, 228.
[6] R. Pöttgen, *Z. Naturforsch.* **1994**, *49b*, 1309.
[7] P. Gravereau, F. Mirambet, B. Chevalier, F. Weill, L. Fournès, D. Laffargue, F. Bourée, J. Etourneau, *J. Mater. Chem.* **1994**, *4*, 1893.
[8] D. Niepmann, R. Pöttgen, B. Künnen, G. Kotzyba, *J. Solid State Chem.* **2000**, *150*, 139.
[9] Th. Fickenscher, U. Ch. Rodewald, D. Niepmann, R. Mishra, M. Eschen, R. Pöttgen, *Z. Naturforsch.* **2005**, *60b*, 271.
[10] Ya.M. Kalychak, V. I. Zaremba, V. M. Baranyak, P. Yu. Zavalii, V. A. Bruskov, L. V. Sysa, O. V. Dmytrakh, *Izv. Akad. Nauk SSSR, Neorg. Mater.* **1990**, *26*, 94.
[11] V. A. Derkach, B.Ya. Kotur, *Inorg. Mater.* **1994**, *30*, 928.
[12] F. Fourgeot, B. Chevalier, P. Gravereau, L. Fournès, J. Etourneau, *J. Alloys Compd.* **1995**, *218*, 90.
[13] R. A. Gordon, Y. Ijiri, C. M. Spencer, F. J. DiSalvo, *J. Alloys Compd.* **1995**, *224*, 101.
[14] B. Chevalier, F. Fourgeot, L. Fournès, P. Gravereau, G. Le Caër, J. Etourneau, *Physica B* **1996**, *226*, 283.
[15] R. P. Pinto, M. M. Amado, M. E. Braga, J. B. Sousa, B. Chevalier, D. Laffargue, J. Etourneau, *J. Appl. Phys.* **1996**, *79*, 6355.
[16] B. Chevalier, F. Fourgeot, D. Laffargue, J. Etourneau, F. Bouree, T. Roisnel, *Physica B* **1997**, *230–232*, 195.
[17] F. Fourgeot, B. Chevalier, P. Gravereau, J. Etourneau, *Physica B* **1997**, *230–232*, 256.
[18] R. P. Pinto, M. M. Amado, M. E. Braga, M. M. P. de Azevedo, J. B. Sousa, B. Chevalier, J. Etourneau, *J. Appl. Phys.* **1997**, *81*, 4182.
[19] F. Fourgeot, A. Demourgues, J. Avila, M. C. Asensio, B. Chevalier, *Nucl. Instr. Meth. Phys. Res.* **1997**, *133*, 127.
[20] B. Chevalier, F. Fourgeot, D. Laffargue, P. Gravereau, L. Fournès, J. Etourneau, *J. Alloys Compd.* **1997**, *262–263*, 114.
[21] R. P. Pinto, M. M. Amado, M. E. Braga, Yu. G. Pogorelov, B. Chevalier, J. Etourneau, J. B. Sousa, *J. Magn. Magn. Mater.* **1999**, *196–197*, 710.
[22] B. Chevalier, J. García Soldevilla, J. C. Gómez Sal, J. M. Barandiarán, J. Etourneau, *J. Magn. Magn. Mater.* **1999**, 196–197, 878.
[23] B. Chevalier, J. García Soldevilla, J. I. Espeso, J. Rodríguez Fernández, J. C. Gómez Sal, J. Etourneau, *Physica B* **1999**, 259–261, 44.

[24] D. Laffargue, F. Bourée, B. Chevalier, J. Etourneau, T. Roisnel, *Physica B* **1999**, *259–261*, 46.
[25] B. Penc, M. Hofmann, M. Ślaski, P. Starowicz, A. Szytuła, *J. Alloys Compd.* **1999**, *282*, 8.
[26] S. F. Matar, A. Mavromaras, *J. Solid State Chem.* **2000**, *149*, 449.
[27] P. Kumar, N. K. Singh, K. G. Suresh, A. K. Nigam, *Phys. Rev. B* **2008**, *77*, 184411.
[28] L. Romaka, M. Konyk, V. V. Romaka, N. Melnychenko, P. Rogl, *J. Alloys Compd.* **2008**, *454*, 136.
[29] V. V. Romaka, P. Rogl, L. Romaka, N. Melnychenko, *J. Alloys Compd.* **2009**, *485*, 275.
[30] L. Romaka, V. V. Romaka, Yu. Stadnyk, P. Demchenko, *J. Alloys Compd.* **2010**, *505*, 70.
[31] V. V. Romaka, L. Romaka, *J. Alloys Compd.* **2011**, *509*, 4530.
[32] L. Romaka, Yu. Dovgalyuk, V. V. Romaka, I. Lototska, Yu. Stadnyk, *Intermetallics* **2012**, *29*, 116.
[33] R. Pöttgen, Th. Gulden, A. Simon, *GIT Labor-Fachzeitschrift* **1999**, *43*, 133.
[34] K. Yvon, W. Jeitschko, E. Parthé, *J. Appl. Crystallogr.* **1977**, *10*, 73.
[35] Ya.V. Galadzhun, R. Pöttgen, *Z. Anorg. Allg. Chem.* **1999**, *625*, 481.
[36] G. M. Sheldrick, SHELXL-97, Program for the Refinement of Crystal Structures, University of Göttingen, Göttingen (Germany) **1997**.
[37] G. M. Sheldrick, *Acta Crystallogr.* **2008**, *A64*, 112.
[38] Y. Zhuang, H. Deng, J. Liu, Q. Yao, *J. Alloys Compd.* **2004**, *363*, 223.
[39] J. Donohue, *The Structures of the Elements,* Wiley, New York **1974**.
[40] J. Emsley, *The Elements*, Oxford University Press, Oxford **1999**.
[41] M. Pani, F. Merlo, M. L. Fornasini, *Z. Kristallogr.* **2002**, *217*, 415.
[42] R. M. Rykhal', O. S. Zarechnyuk, V. S. Protasov, *Dopov. Akad. Nauk. Ukr. RSR, Ser. A* **1985**, 72.
[43] S. Schoolaert, W. Jung, *Z. Anorg. Allg. Chem.* **2002**, *628*, 1806.
[44] S. L. Samal, J. D. Corbett, *Z. Anorg. Allg. Chem.* **2012**, *638*, 1963.
[45] F. Stadler, Th. Fickenscher, R. Pöttgen, *Z. Naturforsch.* **2001**, *56b*, 1241.
[46] C. Kollmar, R. Hoffmann, *Inorg. Chem.* **1990**, *29*, 2466.
[47] J. F. Riecken, G. Heymann, W. Hermes, U. Ch. Rodewald, R.-D. Hoffmann, H. Huppertz, R. Pöttgen, *Z. Naturforsch.* **2008**, *63b*, 695.
[48] G. Heymann, J. F. Riecken, S. Rayaprol, S. Christian, R. Pöttgen, H. Huppertz, *Z. Anorg. Allg. Chem.* **2007**, *633*, 77.
[49] C. P. Sebastian, G. Heymann, B. Heying, U. Ch. Rodewald, H. Huppertz, R. Pöttgen, *Z. Anorg. Allg. Chem.* **2007**, *633*, 1551.
[50] J. F. Riecken, G. Heymann, T. Soltner, R.-D. Hoffmann, H. Huppertz, D. Johrendt, R. Pöttgen, *Z. Naturforsch.* **2005**, *60b*, 821.